Journal of Fluids and Structures 17 (2003) 1213–1236

JOURNAL OF FLUIDS AND STRUCTURES

www.elsevier.nl/locate/jnlabr/yjfls

Simulation of turbulent flows around a circular cylinder using nonlinear eddy-viscosity modelling: steady and oscillatory ambient flows

M. Saghafian[a,1], P.K. Stansby[b,*], M.S. Saidi[a], D.D. Apsley[b]

[a] *Department of Mechanical Engineering, Isfahan University of Technology, Isfahan, Iran*
[b] *Manchester Centre for Civil and Construction Engineering, UMIST, Manchester, UK*

Received 13 September 2001; accepted 19 April 2003

Abstract

Steady incident flow past a circular cylinder for sub- to supercritical Reynolds number has been simulated as an unsteady Reynolds-averaged Navier–Stokes (RANS) equation problem using nonlinear eddy-viscosity modelling assuming two-dimensional flow. The model of Craft et al. (Int. J. Heat Fluid Flow 17 (1996) 108), with adjustment of the coefficients of the 'cubic' terms, predicts the drag crisis at a Reynolds number of about 2×10^5 due to the onset of turbulence upstream of separation and associated changes in Strouhal number and separation positions. Slightly above this value, at critical Reynolds numbers, drag is overestimated because attached separation bubbles are not simulated. These do not occur at supercritical Reynolds numbers and drag coefficient, Strouhal number and separation positions are in approximate agreement with experimental measurements (which show considerable scatter). Fluctuating lift predictions are similar to sectional values measured experimentally for subcritical Reynolds numbers but corresponding measurements have not been made at supercritical Reynolds numbers. For oscillatory ambient flow, in-line forces, as defined by drag and inertia coefficients, have been compared with the experimental values of Sarpkaya (J. Fluid Mech. 165 (1986) 61) for values of the frequency parameter, $\beta = D^2/\nu T$, equal to 1035 and 11240 and Keulegan–Carpenter numbers, $\mathrm{KC} = U_0 T/D$, between 0.2 and 15 (D is cylinder diameter, ν is kinematic viscosity, T is oscillation period, and U_0 is the amplitude of oscillating velocity). Variations with KC are qualitatively reproduced and magnitudes show best agreement when there is separation with a large-scale wake, for which the turbulence model is intended. Lift coefficients, frequency and transverse vortex shedding patterns for $\beta = 1035$ are consistent with available experimental information for $\beta \approx 250 - 500$. For $\beta = 11240$, it is predicted that separation is delayed due to more prominent turbulence effects, reducing drag and lift coefficients and causing the wake to be more in line with the flow direction than transverse to it. While these oscillatory flows are highly complex, attached separation bubbles are unlikely and the flows probably two dimensional.

1. Introduction

The flow past a circular cylinder has received considerable attention over the years but numerical modelling from sub- to supercritical Reynolds numbers has yet to be undertaken successfully. While unsteady 2-D laminar computations are now routine, 3-D computations, or direct numerical simulation (DNS), require massive computer resources which

*Corresponding author.
E-mail address: p.k.stansby@umist.ac.uk (P.K. Stansby).
[1] Visiting Manchester Center for Civil and Construction Engineering.

0889-9746/03/$ - see front matter
doi:10.1016/S0889-9746(03)00066-5

increase markedly as Reynolds number increases and, to date, results for values up to about 500 have been achieved, e.g., Karniadakis and Triantafyllou (1992). However, Reynolds-averaged Navier–Stokes (RANS) turbulence closures may be used to compute flows at very high Reynolds numbers.

Turbulence models are essentially a pragmatic representation of small-scale, high-frequency fluctuations embedded within a mean or (as in this case) slowly varying 'large-scale' flow. Three levels of modelling are commonly adopted: the Boussinesq eddy-viscosity assumption based on the laminar stress–strain relation with 'viscosity' adjusted to account for turbulent mixing; simulation of the RANS equations with the six components of Reynolds stress and a dissipation rate (or other length-scale determining variable) defined by their transport equations; and so-called large-eddy simulation (LES) where 'slowly varying' components are assumed to extend down to the mesh size where subgrid models, based on the eddy-viscosity concept, are applied. While there are obvious limitations and different weaknesses in all approaches, there have been notable successes, e.g., the mixing length concept for eddy viscosity (Prandtl, 1927) has been remarkably successful for simple boundary-layer flows and the $k-\varepsilon$ model for eddy viscosity defines the 'mean' flow properties accurately for attached unsteady boundary layers, e.g., Letherman et al. (2000), where k is turbulence kinetic energy and ε is its dissipation rate. However, when separation occurs the capabilities of different turbulence models are less certain. LES is a 3-D, and hence a very computationally demanding, approach which is probably realistic away from a solid boundary, but close to a boundary has all the limitations of a simple eddy-viscosity formulation. Reynolds stress transport modelling is theoretically appealing and progress has been made with near-wall formulations, e.g., Craft et al. (2001). However, numerical stability is often problematic and, with seven transport equations and often a small time step for stability, it can also be very computationally demanding. To avoid these latter problems, nonlinear eddy-viscosity modelling has been proposed, as reviewed, for example, in Apsley et al. (1997). Reynolds stresses are defined by algebraic formulae which depend on nonlinear combinations of mean strain and vorticity as well as k and ε. In this way some of the weaknesses of previous linear eddy-viscosity models are avoided and important, well-defined, effects are represented, at least qualitatively, with coefficients which may be tuned for particular applications. Nonlinear models are thus made to mimic the physics of turbulence, by means of mathematical artefacts and calibration. The underlying philosophy remains that of the mixing-length approach. In relation to the flows of interest here, particular weaknesses of the linear eddy-viscosity models relate to: turbulence production near stagnation, insensitivity to curvature, separation on curved surfaces and often poor prediction of transition.

Lu et al. (1997) have applied LES to steady incident flow past a circular cylinder with a Reynolds number of 10^4, giving good force and Strouhal number predictions. The Smagorinsky subgrid model was used, unusually without special treatment close to a wall. Oscillatory flow was also investigated for $\beta = 1035$ and $KC \leqslant 10$ and in-line force was in approximate agreement with the experiments of Sarpkaya (1986). Breuer (1998) applied LES to steady flow past a circular cylinder at a Reynolds number of 3900 and found detailed results to be dependent on numerical details, notably the choice of advection scheme with central differencing being recommended. LES for square cylinders has received much more attention, but again results appear sensitive to numerical details, e.g., Rodi et al. (1996), Murakami and Iizuka (1999), although the square cylinder has the physical advantage that upstream separation is fixed by sharp corners. RANS solvers have also been widely applied to square cylinders with full Reynolds-stress transport equations giving better results than linear or nonlinear eddy-viscosity modelling (Rodi et al., 1996). Application of RANS solvers to the circular cylinder has been less common, but results from Celik and Shaffer (1995) using linear $k-\varepsilon$ models show poor agreement with experiment.

In this paper, nonlinear eddy-viscosity models are applied to the circular cylinder case for the first time to our knowledge, although corresponding applications have been made for other flows, e.g., unsteady compressible flows around lifting aerofoils (Barakos and Drikakis, 2000). Assuming two-dimensional large-scale flow, three turbulence models are applied: those of Speziale (1987), Craft et al. (1996) and Lien et al. (1996). The model of Craft et al. seems most appropriate and some (limited) adjustments are made to coefficients to fit the experimental data. The models are applied through a range of Reynolds numbers, from 10^3 to10^7, where flows vary from: subcritical Reynolds numbers with laminar separation and transition to turbulence in the separated shear layers; to critical Reynolds numbers with laminar separation and turbulent transition sufficiently close to form re-attachment bubbles before turbulent separation; to supercritical Reynolds numbers with turbulent separation and a vortex-shedding wake (as for subcritical but with a higher Strouhal number).

These wakes have a spanwise cellular structure where a cell contains vorticity predominantly parallel to or slightly inclined to the cylinder axis. Streamwise vorticity connects to the cell boundaries in a complex manner, investigated in great detail for Reynolds numbers less than 1000, e.g., Williamson (1996). Vortex inclination had previously been estimated through hot-wire measurements for a Reynolds numbers of 3600 by Stansby (1974), investigating the effect of end plates, see also Szepessy (1993). The cells may be stationary or fluctuating with a spanwise extent which is typically several diameters but dependent on end conditions and Reynolds number. Vortex shedding is thus not in phase along the span and the fluctuating lift is highly dependent on the spanwise length over which force is measured. The mean

drag coefficient and the Strouhal number, however, show little dependence. Local or sectional lift forces have recently been obtained by Norberg (2001) for subcritical Reynolds numbers and are most suited for comparison with a 2-D model, although vortex inclination will of course reduce force magnitude to some degree.

It is worth mentioning that one of the most important effects of unsteady wake flows relates to flexible cylinders causing 'vortex-induced vibrations' (or VIV) which correlates the larger scale flow structures along the span, making the flow nearly 2-D. Thus, while the flow around a stationary cylinder is an inevitable first step, allowing dynamic response probably makes 2-D simulations of more direct value.

The model of Craft et al. (1996) is also applied to oscillatory flows and forces are compared with the experimental results of Sarpkaya (1986) for $\beta = 1035$ and 11240. These separated and vortex-shedding flows are clearly complex and turbulent but are thought to be predominantly 2-D without attached separation bubbles and so are well suited for this form of modelling.

2. Mathematical formulation

The RANS equations can be written for incompressible flow in tensor notation as follows:

$$\frac{\partial U_i}{\partial x_i} = 0, \tag{1}$$

$$\frac{\partial U_i}{\partial t} + U_j \frac{\partial U_i}{\partial x_j} = -\frac{1}{\rho}\frac{\partial P}{\partial x_i} + \frac{\partial}{\partial x_j}\left(\nu \frac{\partial U_i}{\partial x_j} - \overline{u_i u_j}\right). \tag{2}$$

Upper case denotes ensemble-mean quantities and lower case fluctuating or turbulence quantities; P is pressure and ρ is density. An overbar is used to denote Reynolds averaging. The momentum equations are not a closed set and turbulence models are used to model the turbulent or Reynolds stresses ($-\overline{u_i u_j}$). Linear and nonlinear $k-\varepsilon$ models are now defined.

2.1. Linear model

The linear stress–strain relation is defined as follows:

$$\overline{u_i u_j} = -2\nu_t S_{ij} + \tfrac{2}{3} k \delta_{ij}, \tag{3}$$

where δ_{ij} is the Kronecker delta, S_{ij} is the mean stress tensor (defined in Eq. (11) below) and eddy viscosity ν_t is defined by

$$\nu_t = C_\mu f_\mu \frac{k^2}{\tilde{\varepsilon}} \tag{4}$$

with coefficients C_μ and f_μ given in Table 1 (for the various models used). k is the turbulent kinetic energy and $\tilde{\varepsilon}$ is the homogeneous part of the dissipation rate ε. Transport equations for k and $\tilde{\varepsilon}$ are

$$\frac{\partial k}{\partial t} + U_j \frac{\partial k}{\partial x_j} = \frac{\partial}{\partial x_j}\left(\left(\nu + \frac{\nu_t}{\sigma_k}\right)\frac{\partial k}{\partial x_j}\right) + P^k - \varepsilon, \tag{5}$$

$$\frac{\partial \tilde{\varepsilon}}{\partial t} + U_j \frac{\partial \tilde{\varepsilon}}{\partial x_j} = \frac{\partial}{\partial x_j}\left(\left(\nu + \frac{\nu_t}{\sigma_\varepsilon}\right)\frac{\partial \tilde{\varepsilon}}{\partial x_j}\right) + C_{\varepsilon 1} f_1 \frac{\tilde{\varepsilon}}{k} P^k - C_{\varepsilon 2} f_2 \frac{\tilde{\varepsilon}^2}{k} + E, \tag{6}$$

where E is defined in Table 1 and the turbulent kinetic energy production rate is

$$P^k = -\overline{u_i u_j}\frac{\partial U_i}{\partial x_j} = 2\nu_t S_{ij} S_{ij}. \tag{7}$$

Application of the Boussinesq assumption, Eq. (3), gives

$$P^k = \nu_t\left(\frac{\partial U_i}{\partial x_j} + \frac{\partial U_j}{\partial x_i}\right)\frac{\partial U_i}{\partial x_j}. \tag{8}$$

The homogeneous and inhomogeneous parts of the dissipation rate are summed together

$$\varepsilon = \tilde{\varepsilon} + D. \tag{9}$$

In high-Reynolds number $k-\varepsilon$ models $f_\mu = 1,\ D = E = 0,\ \varepsilon = \tilde{\varepsilon}$.

Table 1
Coefficients for the turbulence models

	Launder–Sharma LS	Speziale	Craft–Launder–Suga (CLS)	Lien–Chen–Leschziner (LCL)
$C_{\varepsilon 1}$	1.44	1.44	1.44	1.44
$C_{\varepsilon 2}$	1.92	1.92	1.92	1.92
σ_k	1.0	1.0	1.0	1.0
σ_ε	1.3	1.3	1.3	1.3
C_μ	0.09	0.09	$\frac{0.3}{1+0.35\eta^{3/2}}(1-\exp(-0.36e^{0.75\eta}))$	$\frac{2/3}{1.25+\bar{S}+0.9\bar{\Omega}}$
C_1	0	0.054	$-0.4C_\mu f_\mu$	$3f_\mu/(1000+\bar{S}^3)$
C_2	0	0.054	$0.4C_\mu f_\mu$	$15f_\mu/(1000+\bar{S}^3)$
C_3	0	0	$1.04C_\mu f_\mu$	$19f_\mu/(1000+\bar{S}^3)$
C_4	0	0	$80C_\mu^3 f_\mu$	$80C_\mu^3 f_\mu$
C_5	0	0	0	0
C_6	0	0	$-40C_\mu^3 f_\mu$	$-16C_\mu^3 f_\mu$
C_7	0	0	$40C_\mu^3 f_\mu$	$16C_\mu^3 f_\mu$
Low-Re terms				
f_μ	$\exp\left(\frac{-3.4}{(1+R_t/50)^2}\right)$	—	$1-\exp[-(R_t/90)^{1/2}-(R_t/400)^2]$	$\frac{1-\exp(-0.0198y^*)}{(1+2\kappa/C_\mu^{3/4}y^*)^{-1}}$
f_1	1	—	1	1
f_2	$1-0.3\exp(-R_t^2)$	—	$1-0.3\exp(-R_t^2)$	$1-0.3\exp(-R_t^2)$
D	$2\nu\left(\frac{\partial k^{1/2}}{\partial x_i}\right)^2$	—	$2\nu\left(\frac{\partial k^{1/2}}{\partial x_i}\right)^2$ $YAP, (R_t \leqslant 250)$ $0.0022\frac{\tilde{S}\nu_t k^2}{\tilde{\varepsilon}}\left(\frac{\partial^2 U_i}{\partial x_j \partial x_k}\right)^2 + YAP,$	0
E	$2\nu\nu_t\left(\frac{\partial^2 U_i}{\partial x_j \partial x_k}\right)^2$	—	$(R_t \geqslant 250)$	$C_{\varepsilon 2}f_2\frac{\varepsilon^1\varepsilon}{k}\exp(-0.00375y^{*^2})$

$R_t = k^2/\nu\tilde{\varepsilon}$, $y^* = y_n k^{1/2}/\nu$ y_n is distance from the wall.
$\tilde{S} = (k/\varepsilon)\sqrt{2S_{ij}S_{ij}}$, $\tilde{\Omega} = (k/\varepsilon)\sqrt{2\Omega_{ij}\Omega_{ij}}$, $\eta = \mathrm{Max}(\tilde{S}, \tilde{\Omega})$.
$YAP = \mathrm{Max}\big(0.83(\gamma-1)\gamma^2(\tilde{\varepsilon}^2/k), 0\big)$, $\gamma = k^{3/2}/c_l\tilde{\varepsilon}y_n$, $c_l = 2.5$, $\varepsilon^1 = (k^{3/2}/\kappa y_n)(C_\mu^{3/4} + 2\kappa/y^*)$.

2.2. Nonlinear models

In quadratic and cubic eddy-viscosity models, the stress–strain relationship can be written in the following form (Craft et al., 1996):

$$\begin{aligned}\overline{u_i u_j} = {} & \frac{2}{3}k\delta_{ij} - 2C_\mu f_\mu \frac{k^2}{\tilde{\varepsilon}} S_{ij} \\ & + c_1 \frac{k^3}{\tilde{\varepsilon}^2}\left(S_{ik}S_{jk} - \frac{1}{3}S_{kl}S_{kl}\delta_{ij}\right) + c_2 \frac{k^3}{\tilde{\varepsilon}^2}(S_{ik}\Omega_{jk} + S_{jk}\Omega_{ik}) + c_3 \frac{k^3}{\tilde{\varepsilon}^2}\left(\Omega_{ik}\Omega_{jk} - \frac{1}{3}\Omega_{kl}\Omega_{kl}\delta_{ij}\right) \\ & + c_4 \frac{k^4}{\tilde{\varepsilon}^3}(S_{ik}\Omega_{jl} + S_{jk}\Omega_{il})S_{kl} + c_5 \frac{k^4}{\tilde{\varepsilon}^3}\left(\Omega_{ik}\Omega_{kl}S_{lj} + \Omega_{jk}\Omega_{kl}S_{li} - \frac{2}{3}\Omega_{kl}S_{lm}\Omega_{mk}\delta_{ij}\right) \\ & + c_6 \frac{k^4}{\tilde{\varepsilon}^3}S_{kl}S_{kl}S_{ij} + c_7 \frac{k^4}{\tilde{\varepsilon}^3}\Omega_{kl}\Omega_{kl}S_{ij}. \end{aligned} \tag{10}$$

Mean strain and vorticity tensors are defined by

$$S_{ij} = \frac{1}{2}\left(\frac{\partial U_i}{\partial x_j} + \frac{\partial U_j}{\partial x_i}\right), \quad \Omega_{ij} = \frac{1}{2}\left(\frac{\partial U_i}{\partial x_j} - \frac{\partial U_j}{\partial x_i}\right). \tag{11}$$

Table 1 displays coefficients and terms for the linear Launder and Sharma (1974) and the three nonlinear models of Speziale (1987), Craft et al. (1996) and Lien et al. (1996). The first nonlinear model is quadratic and the other two are cubic. The nonlinear components of Reynolds stresses, Eq. (10), are included in the RANS momentum equations as source terms.

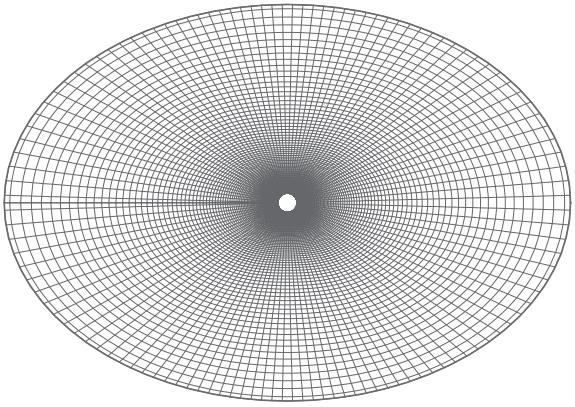

Fig. 1. Computational grid.

3. Numerical solution

The finite-volume approach is applied to discretise the partial differential equations using a body-fitted O-type collocated grid, as shown in Fig. 1. The SIMPLEC pressure-correction algorithm is employed to solve the numerical problem with the Rhie–Chow interpolation scheme for cell-face velocities to prevent nonphysical oscillations in pressure. The popular third-order accurate upwind QUICK scheme is applied to the advective terms in the momentum equations and the lower-order HYBRID scheme in the k and ε transport equations to avoid numerical instability. These, now standard, methods are described, for example, in Ferziger and Peric (1996). At the inflow boundary a uniform velocity U is input, the turbulence kinetic energy is set to a low value, $k/U^2 = 10^{-3}$ or 10^{-4}, with $v_t/v \approx 1.0$. At an outflow boundary the convective boundary condition may be applied for each variable:

$$\frac{\partial \varphi_i}{\partial t} + U_\infty \frac{\partial \varphi_i}{\partial x} = \frac{\partial \varphi_\infty}{\partial t}. \tag{12}$$

This is generally applied and is particularly useful in steady onset flow as it minimises the upstream effect of the wake crossing the downstream boundary, e.g., see Sani and Gresho (1994). Grid-independent results were obtained with 140×120 grid points in the r and θ directions, respectively. The dimension of the domain in the flow direction is $30D$ and in the transverse direction is $21D$. Grid independence (or numerical convergence) is determined here from the force values, which are the main focus of this paper. While the drag coefficient and the Strouhal number (both defined below) are relatively insensitive parameters, the fluctuating lift coefficient is quite sensitive to numerical details; e.g., see Stansby and Slaouti (1993). Results with a 102×102 mesh were generally very close and further limited tests with a 162×162 mesh gave almost identical results to the 140×120 mesh. It may be noted that the 162×162 mesh has been used with LES which requires definition of smaller scales than the present approach. The radial cell size at the surface (δ) is a maximum, $\delta_{\max}$, in the flow direction ($\theta = 0^\circ$, 180°) and a minimum, $\delta_{\min}$, in the transverse direction ($\theta = 90^\circ$, 270°) where $\delta_{\min} = 0.46\delta_{\max}$. This reduces the variation of $y^+ = \delta u^+/v$, where u^+ is the friction velocity, around the cylinder in the surface cell which is desirable for turbulence modelling. In these applications $\delta_{\max}/D$ is varied from 0.001 (for low Reynolds numbers) to 0.0001 (for high Reynolds numbers). This gives a maximum y^+ of about unity. Different values for nondimensional time step, $\delta t U_0/D$, (0.005, 0.01, 0.02 and 0.03) were tested and 0.02 was usually selected (δt is time step and U_0 is the maximum incident velocity).

4. Results

4.1. Steady ambient flow

Four turbulence models were initially applied to steady ambient flow around a cylinder: the linear Launder–Sharma (LS) model (probably the industry-standard, low-Reynolds-number model); the nonlinear Speziale model, with quadratic terms; the nonlinear Craft, Launder, Suga (CLS) model, with cubic terms; and the Lien, Chen and Leschziner (LCL) model, also with cubic terms. Coarse predictive quality was assessed through comparison of the drag coefficient,

C_D = (Drag force)/($\frac{1}{2}\rho U^2 D$), and the Strouhal number, $S = f_L D/U$, where f_L is the lift frequency, with the experiments of Schewe (1983). The fundamental limitations of the LS model are well known, notably the overprediction of turbulence near stagnation, generating turbulent boundary layers upstream of separation at Reynolds numbers well below the critical values. The CLS model was most effective, importantly predicting transition to turbulent separation at a Reynolds number, Re(= UD/v)$\approx 3\times10^5$. The cubic terms with coefficients c_6 and c_7 are necessary to account for curvature effects and the low-Reynolds number elements in the CLS model are, in particular, set up to resolve flows with complex strain and sensitivity to viscous effects, as occur in these problems. Tuning the cubic coefficients has previously been suggested by Lien et al. (1996). Reducing these values by 60% (as suggested by Lien et al. with reference to separation from a curved surface) produced the best overall agreement with experiment and the CLS model with this modification is used henceforth. Note that this modification only affects curved flow; in simple shear the last two nonlinear terms cancel out.

The dependence of C_D, S and $C_{L\,\mathrm{r.m.s.}}$ on Re is shown in Fig. 2; C_D represents the mean drag coefficient and C_L is the lift force coefficient normalised in the same way as drag. At this stage it is also thought useful to catalogue the effect of the different terms in the CLS model on C_D and S and this is done in Table 2. Linear (case A) and linear/quadratic (case B) terms are seen to give C_D values which are far too high. The addition of standard cubic terms (case C) causes C_D to be too low, while reducing cubic terms by 60% (case D) gives much improved agreement.

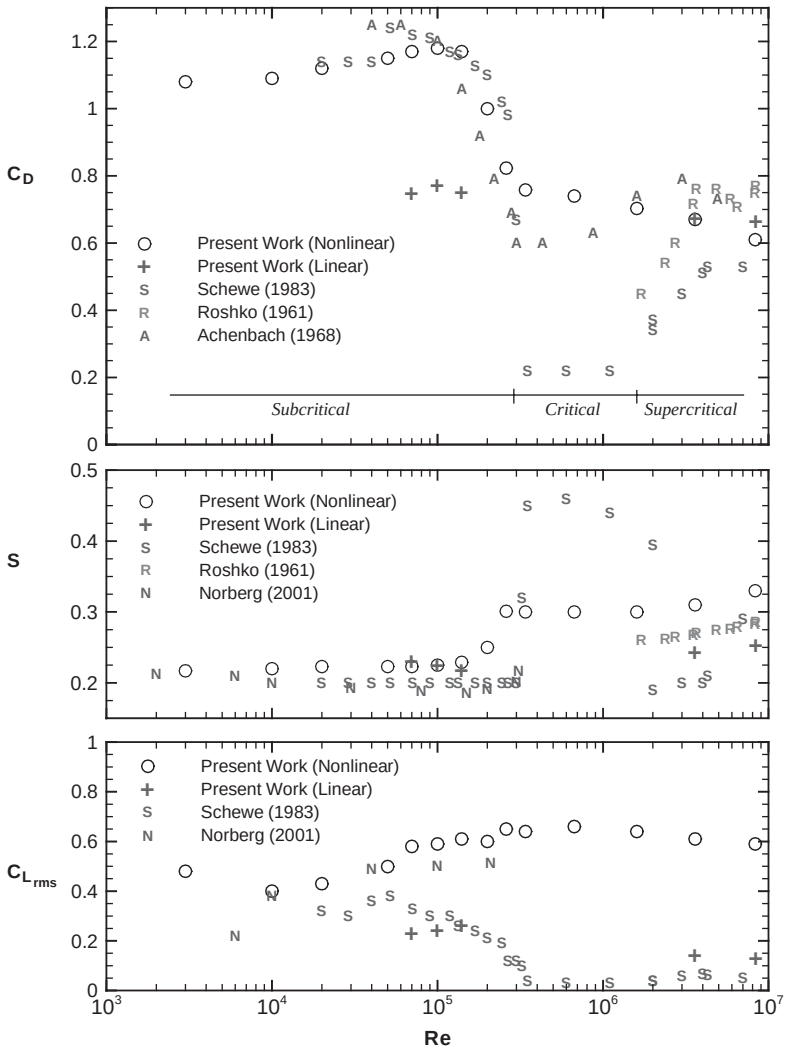

Fig. 2. Variation of mean drag coefficient, Strouhal number and r.m.s. lift coefficient with Reynolds number, comparing the nonlinear (modified) CLS model and the linear LS model with experimental data.

Table 2
Results from the CLS model

	Case A	Case B	Case C	Case D
$\mathrm{Re} = 1.0 \times 10^4$				
C_D	1.5	1.55	0.95	1.09
S	0.249	0.244	0.217	0.22
$\mathrm{Re} = 1.0 \times 10^5$				
C_D	1.65	1.832	0.93	1. 18
S	0.249	0.25	0.21	0.225
$\mathrm{Re} = 1.4 \times 10^5$				
C_D	1.55	1.82	0.92	1.17
S	0.248	0.25	0.21	0.227
$\mathrm{Re} = 3.4 \times 10^5$				
C_D	0.89	—	0.64	0.76
S	0.29	—	0.16	0.301
$\mathrm{Re} = 3.6 \times 10^6$				
C_D	0.45	0.64	0.41	0.67
S	0.27	0.29	0.1	0.31

Case A: Using linear terms of the models.
Case B: Using linear terms of the models.
Case C: Using all terms of the model.
Case D: Using all linear and quadratic and terms, but $C_6 = -16C_\mu^3 f_\mu$ and $C_7 = 16C_\mu^3 f_\mu$.

It is shown in Fig. 2 that the very small C_D values at critical Reynolds numbers, measured by Schewe (1983), are not predicted. The model does not simulate attached separation bubbles, resulting from laminar separation with transition just downstream, causing turbulent re-attachment which is then followed by turbulent separation forming shear layers which interact to form the wake. In the computations the boundary layers at separation simply become turbulent without reattachment at $\mathrm{Re} \approx 2 \times 10^5$. This coincides with a jump in Strouhal number from about 0.22 to 0.3. In Schewe's experiments S becomes high in the critical range before reverting to about 0.3 in the supercritical range. The predicted C_D variation is in fact in quite close agreement with the results of Achenbach (1968), although less so with the earlier results of Roshko (1961) which show similar trends to Schewe. It seems possible that Achenbach's results were affected by small surface imperfections or incident turbulence disturbing the sensitive re-attachment process. Values from the linear LS model are shown in this figure as a reference for interest. The differences in the results of Schewe, Achenbach and Roshko are clearly seen in the Reynolds number range 2×10^5–5×10^6.

While there is approximate agreement in Strouhal numbers between experiment and the modified CLS model at subcritical and supercritical Reynolds numbers, comparison of fluctuating lift is less straightforward, as discussed above. The values of $C_{L\,\mathrm{r.m.s.}}$ from the model are however approximately equal to or slightly greater than the measurements of sectional force for subcritical Reynolds numbers (Norberg, 2001) (except at Reynolds number of 6000), but change little as Reynolds number increases to critical and supercritical values. Unfortunately, Norberg's values only extend to $\mathrm{Re} \approx 2 \times 10^5$. $C_{L\,\mathrm{r.m.s.}}$ values from Schewe measured on a span of ten diameters are less than Norberg's sectional values at subcritical Reynolds numbers, as would be expected, and become very small in the critical and supercritical ranges. A better appraisal of predicted $C_{L\,\mathrm{r.m.s.}}$ values at supercritical Reynolds numbers would require experiments of the kind undertaken by Norberg (2001) for subcritical Reynolds numbers. It is worth mentioning, however, that there is visual evidence of 'strong' vortex shedding at $\mathrm{Re} \approx 2 \times 10^6$ from a vibrating pile in an estuary, where vortex shedding is expected to be well correlated, shown in a photograph of the water surface (CIRIA Report UR8, 1977).

Examples of lift and drag variation with time are shown in Fig. 3 for four Reynolds numbers from subcritical to supercritical. The near-sinusoidal lift variation is seen, with a much smaller drag fluctuation at twice the lift frequency superimposed on the mean value. Fig. 4 shows mean surface pressure coefficient distributions around the cylinder from the modified CLS model and the LS model for comparison, with available experimental measurements and some LES

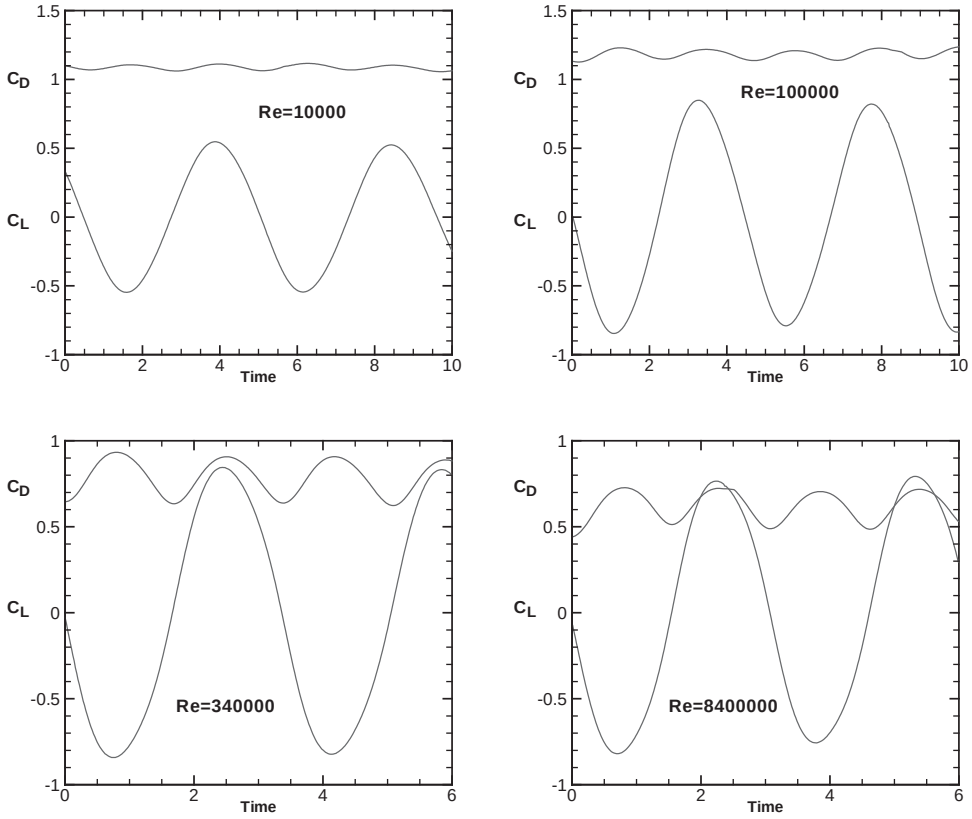

Fig. 3. The variation of drag and lift force coefficients from the modified CLS model with (nondimensional) time for four Reynolds numbers.

modelling. While there is scatter in the experimental values, there should perhaps be most concern about the results for $Re = 8.4 \times 10^6$. Here we only have the experimental results of Roshko which show remarkably good agreement with the LS model with its well-known limitation of overproduction of turbulence near stagnation. The modified CLS model shows a much higher suction pressure (negative pressure) around $\theta \approx \pm 90^\circ$ and a lower base suction, except close to $\theta \approx 180^\circ$. The latter effect has been observed previously to be due to an artificially 2-D wake with rolling up of vortices close to the cylinder causing high velocities (Smith and Stansby, 1989). Given the above limitation of the LS model, this does suggest that Roshko's experiments might also have experienced extraneous turbulence effects, either from a slightly rough surface or free-stream turbulence. With such a small boundary-layer thickness, tiny surface roughness could be significant.

It is of interest to compare the ratio of friction drag to total drag for comparison with the experiments of Achenbach. Fig. 5 shows generally good agreement, except for supercritical Reynolds numbers where the experimental values are much lower than those from the modified CLS model. This again suggests that roughness in the experiments might be an issue. Fig. 6 shows the variation of mean separation positions (defined by zero shear stress) with Reynolds number. The effect of turbulence at separation is clearly seen at $Re \approx 2 \times 10^5$, and the effect of the attached separation bubbles is obviously missing in the model results. The differences at critical Reynolds numbers relate to the uncertainties mentioned above.

Finally, it is instructive to show streamline and turbulence energy contours for the three Reynolds-number regimes, relating to Figs. 3 and 4. Fig. 7a shows a subcritical case for $Re = 10^5$ with the modified CLS model and Fig. 7b shows results with the LS model where the erroneous turbulence upstream of separation is clearly visible. The delayed separation with the modified CLS model is shown in Figs. 7c and d for $Re = 3.4 \times 10^6$ and 8.4×10^6. Vigorous vortex shedding for the supercritical case is clearly seen in Fig. 7d. The attached turbulent boundary layer in the last two cases is so thin that it is hardly visible. The magnitude of turbulence energy within an eddy is seen to decrease as it moves downstream.

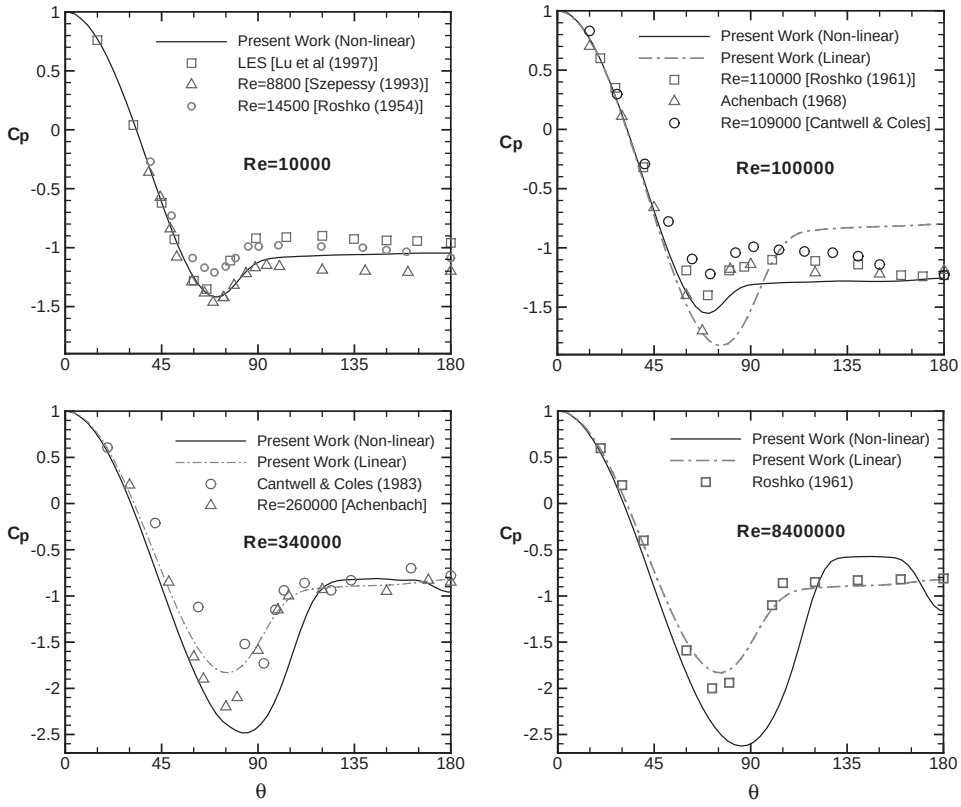

Fig. 4. Pressure coefficient distributions for $Re = 10^4$, $Re = 10^5$, $Re = 3.4 \times 10^5$, and $Re = 8.4 \times 10^6$, comparing the nonlinear (modified) CLS model and linear LS model with experimental data.

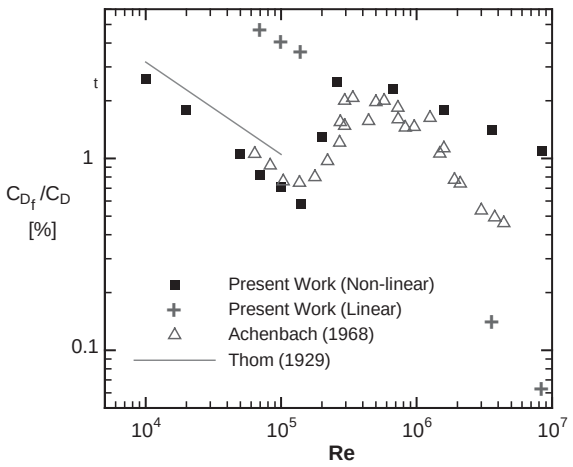

Fig. 5. Variation of the ratio of frictional drag to total drag with Reynolds number.

4.2. Oscillatory ambient flow

Oscillatory, uniform ambient flows around cylinders have received much attention in recent years as an idealisation of wave flows around cylinders. Early experimental work of Keulegan and Carpenter (1958) caused an important defining parameter to be called the Keulegan–Carpenter number, $KC = U_0 T/D$, for sinusoidal flows of velocity

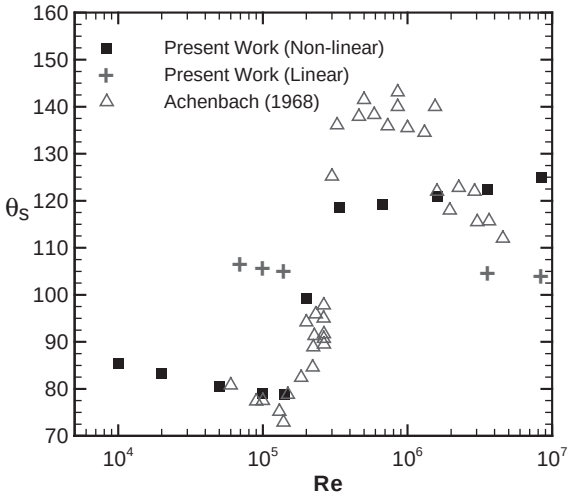

Fig. 6. Variation of the position of separation with Reynolds number.

$U = U_0 \sin(2\pi t/T)$. This is also equal to $2\pi a/D$, where a is the amplitude of particle motion. Subsequently, advantage has been taken of the resonant flow in U-tubes to provide uniform oscillatory ambient flows, notably Sarpkaya (1976, 1986) and Obasaju et al. (1988). The flow is further defined by the parameter $\beta = D^2/vT$, rather than the Reynolds number $\mathrm{Re} = U_0 D/v = \mathrm{KC}\beta$ since it only depends on cylinder diameter for a given U-tube.

We are interested here in high β values (greater than 1000 say), relevant to offshore applications, where the flow is predominantly turbulent. Sarpkaya (1986) made a detailed investigation of in-line force for $\beta = 1035$ and 11240 and we compute these cases using the modified CLS model with KC in the range 0.2–20. Force (per unit length) is conventionally defined using the Morison equation, $F = \frac{1}{2}\rho U|U|C_D D + \rho\pi D^2 C_M \dot{U}/4$, where the drag and inertia coefficients, C_D and C_M, respectively, are obtained usually by Fourier analysis. This formula is well known not to represent all aspects of the actual force, but it enables a concise comparison of results to be made since C_D and C_M are only dependent on KC and β. The model is run for several cycles, at least 5 and up to 15, to allow transients to die away, and C_D and C_M are obtained by analysis of the last three cycles. Comparisons with experimental values are shown in Fig. 8. Cross-flow or lift forces, defined by a lift coefficient, $C_L = (\text{Lift force})/(\frac{1}{2}\rho U_0^2 D)$, occur due to flow asymmetry and vortex shedding for $\mathrm{KC} > 4$, but at this stage we concentrate on C_D and C_M. Here C_M is close to the potential-flow value of 2, except when vortex shedding is prominent, for $\mathrm{KC} > 0.7$, say. The C_D variation is dependent only on viscous effects. For $\beta = 1035$, in Fig. 8a, for small $\mathrm{KC} < 0.7$, the experimental C_D values are close to the laminar theory of Wang (1968). For $\mathrm{KC} \approx 0.7$, a three-dimensional mushroom-like instability, known as the Honji instability (Honji, 1981), occurs and is the first stage of transition to turbulence. This causes an increase in C_D as shown in Fig. 8a. However, C_D continues to decrease with KC, up to $\mathrm{KC} \approx 2$, when separated vortical structures become more prominent, remaining almost symmetric up to $\mathrm{KC} \approx 4$, and then becoming asymmetric with increasingly complex vortex shedding structures as KC increases. The model predictions of C_D and C_M are in reasonable agreement with experiment, except for $\mathrm{KC} = 12$ and $\mathrm{KC} < 2$. Clearly such a turbulence model is not intended to represent such effects as Honji instability and there is a smooth transition with KC, with the C_D value approaching the laminar value as KC decreases. At $\mathrm{KC} = 0.5$, the smallest value investigated, C_D is overestimated by 12% and this is due to the turbulence model instigating transition to turbulence at lower KC than in experiments. It should be noted that the turbulence model with nonlinear terms is set up for predominantly steady flows, and ambient flow frequency is proportional to the inverse of KC. Finally, the low C_D prediction for $\mathrm{KC} = 12$ is possibly due to inadequate representation of complex vortex shedding patterns (shown below).

For $\beta = 11240$ in Fig. 8b, experimental values are only available for $\mathrm{KC} > 0.8$, and the variation of C_D and C_M is predicted reasonably by the model. However, the computed values for $\mathrm{KC} < 0.8$ are of interest (and considerable practical importance in relation to hydrodynamic damping). Honji instability would be expected at $\mathrm{KC} \approx 0.6$ but the predicted C_D values are much greater than Wang's laminar values below this value, as would be associated with turbulent flow. While there are no experimental measurements at $\beta = 11240$, there are at $\beta = 20526$ due to Bearman and Russell (1996) and the model was run for this value with $\mathrm{KC} = 0.2$ and 0.4; C_D values of 1.9 and 1.6 were obtained respectively, comparing with experimental values of 2.0–1.2 and 0.8–1.0. It would thus appear that there is prediction

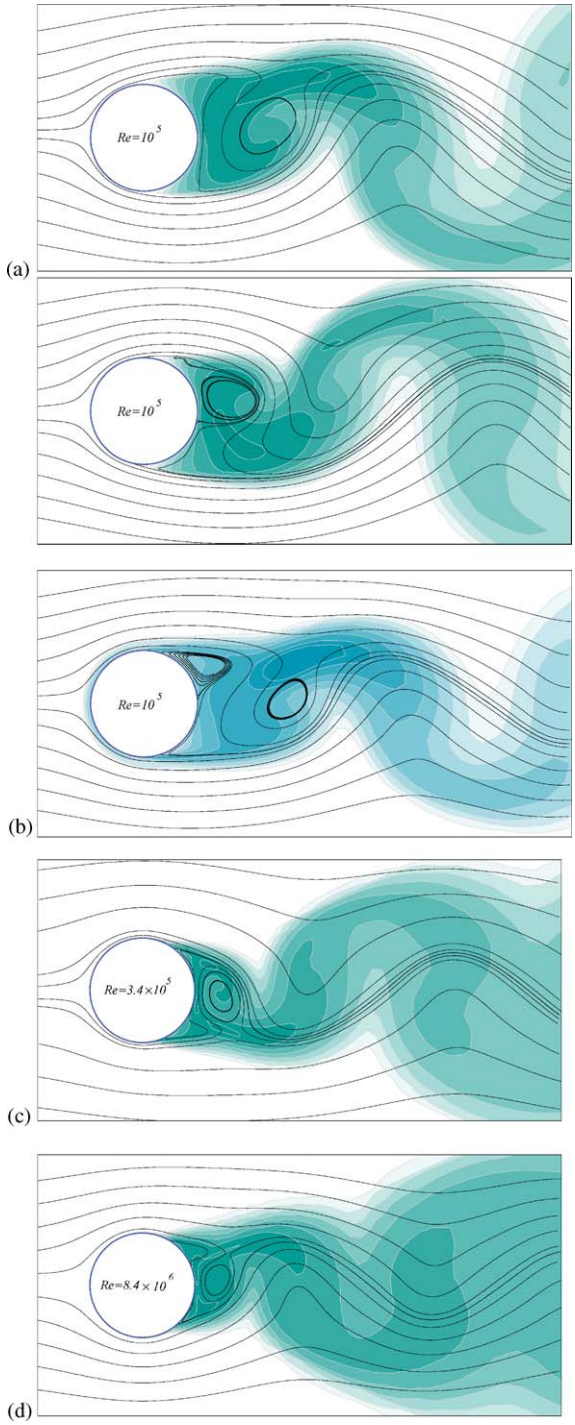

Fig. 7. (a) Streamlines and contours of turbulent kinetic energy (k/U_∞^2) for $\mathrm{Re}=10^5$. (a) At two times in the vortex shedding cycle using the nonlinear modified CLS model. (b) Using the using linear LS model. ($(k/U_\infty^2)_{\min}=5\times10^{-3}$ and $(k/U_\infty^2)_{\max}=0.15$, distribution is not uniform). (c) Streamlines and contours of turbulent kinetic energy (k/U_∞^2) using the nonlinear modified CLS model for a critical Reynolds number. (d) Streamlines and contours of turbulent kinetic energy (k/U_∞^2) using the nonlinear modified CLS model for a supercritical Reynolds number.

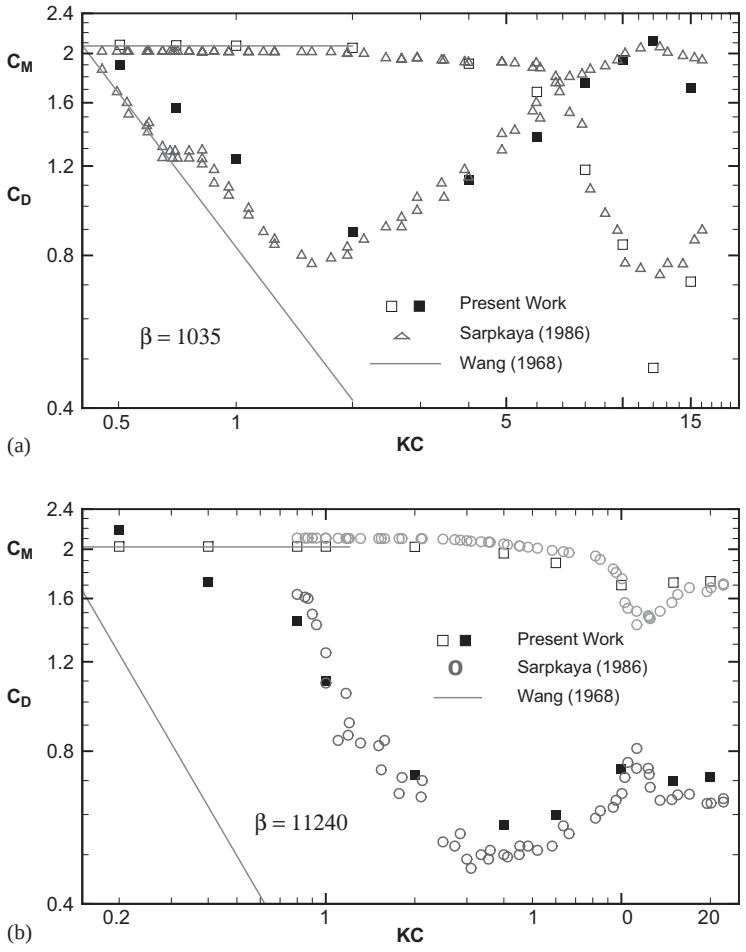

Fig. 8. (a) Variation of drag and inertia coefficients for oscillating flow with KC for $\beta = 1035$, comparing the present modified CLS model with experimental values. (b) Variation of drag and inertia coefficients for oscillating flow with KC for $\beta = 11240$, comparing the present modified CLS model with experimental values.

within experimental scatter at KC = 0.2 when the viscous flow is predominantly that of an attached (curved) boundary layer. However, the limitations in relation to transition prediction, found at $\beta = 1035$, probably mean that C_D will again be overestimated for smaller KC values when the flow eventually becomes laminar. At KC = 0.4, closer to where Honji instability would be expected, C_D is overpredicted, which is again consistent with $\beta = 1035$.

Fluctuating lift was not reported in Sarpkaya (1986), but maximum values of C_L are available in Sarpkaya (1976) for $\beta = 1107$ and computed values are shown in Fig. 9 for $\beta = 1035$ and 11240. The high values for $\beta \approx 1000$ are in broad agreement, and computed values for $\beta = 11240$ are somewhat lower, in keeping with the observed trend at lower β values that C_L decreases as β increases. Lift can be of similar magnitude, or even larger than, in-line force for KC > 7, when vortex shedding effects become prominent. Detailed experimental investigations of vortex shedding behaviour in relation to lift generation have been undertaken, notably by Williamson (1985) with $\beta = 255$ and 510 and by Obasaju et al. (1988) for $\beta = 416$ and 634 (mainly).

Examples of force variation with time are shown in Fig. 10 for KC = 4, 8, 12 and 15 for $\beta = 1035$. The force variation reconstituted from the drag and inertia coefficients derived are also shown to give an indication of the fit obtained by the Morison equation. The in-line force, using the experimentally derived coefficients, is also shown. For KC $\leqslant$ 4 lift is very small, but increases as KC increases. For KC = 8, 12 and 15 the fit of the Morison equation is less close and the lift frequency is at twice the oscillation frequency for KC = 8 and 12. At KC=15, the lift frequency is predominantly three times the oscillation frequency. The effect of vortex shedding on in-line force, not accounted for in Morison's equation, is quite apparent for KC = 8, 12 and 15. For KC = 18 the

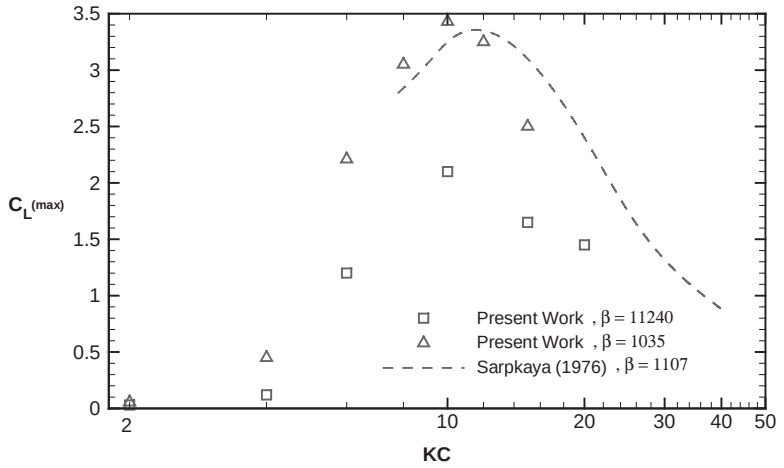

Fig. 9. Variation of maximum lift coefficient in oscillating flow with KC, comparing the present modified CLS model with experiment.

predictions of C_D and C_M (1.1 and 1.3, respectively) were less satisfactory, and this coincides with the flow ceasing to be two dimensional as discussed below.

Plots of streamlines, vorticity and turbulence energy contours are shown in Fig. 11 for the same KC values of 4, 8, 12 and 15 at $\beta = 1035$, for different phases, θ, within a cycle. For KC = 4 there is slight asymmetry, and new vorticity rolling up close to the cylinder is accompanied by weak vortex-pair formation as a residue from the previous half-cycle. The vorticity and turbulence energy remain in a confined area around the cylinder. There is little evidence of vorticity older than two half-cycles. For KC = 8, asymmetry is quite marked, and vorticity crosses from one side of the cylinder to the other. One dominant vortex is shed per half-cycle, with vortex pairing of shed vortices occurring on one side of the cylinder only, forming a transverse wake. A similar process occurs at KC = 12 except that the shed vortices are bigger and the transverse wake wider. KC = 15 is the start of the regime where two dominant vortices are shed per half-cycle with the formation of a vortex pair in each half-cycle on different sides of the cylinder, forming a diagonal wake (more clearly seen at KC = 18). These structures may be related to the lift variations in Fig. 10, reproducing the simple experimental observation that one dominant vortex shed per half-cycle causes a lift frequency of twice the oscillation frequency (Williamson, 1985). At KC = 15, a second vortex in a half-cycle has become more prominent, causing a lift frequency of three times the oscillation frequency. These results are consistent with experiments for a smaller values of β, between about 250 and 500 (Williamson, 1985; Obasaju et al., 1988).

Force variations for $\beta = 11240$ are similar but the lift maxima are smaller and the Morison fit is markedly closer. Examples are shown for KC = 4, 6, 10, 15 and 20 in Fig. 12. The lift variations, for a given KC, have somewhat higher dominant frequencies than those at $\beta = 1035$. Corresponding plots of streamlines, vorticity and turbulence energy contours are shown in Fig. 13. At KC = 4, there is slight asymmetry and a small lift force at the oscillation frequency, rather than at twice with $\beta = 1035$. At KC = 6, one vortex is shed per half-cycle and the lift frequency is twice the oscillation frequency (as for $\beta = 1035$). For KC = 10, however, two prominent vortices are shed in a half-cycle and the vortex pair convection is much more in line with the flow direction than transverse to it, as was the case for $\beta = 1035$. The lift frequency is predominantly at three times the oscillation frequency, although one cycle is rather weaker than the other two. At KC = 15, lift frequency is also predominantly at three times the oscillation frequency and two vortices are shed in a half-cycle, forming a diagonal wake. At KC = 20, three prominent vortices are shed in a half-cycle, causing a lift frequency of four times the oscillation frequency. In all cases vortex pair convection is more in line with the flow direction than for $\beta = 1035$.

At first sight it is perhaps surprising that force prediction for these complex oscillatory flows can be better than for steady ambient flows. However, the careful experimental examination of Obasaju et al. (1988) has shown that the spanwise correlation of lift force is very close to unity for KC < 18, albeit for $\beta = 483$ (although at KC values around 12 lift can be well correlated over different parts of the span but out of phase). For higher KC the correlation deteriorates markedly. We can of course only conjecture that this high correlation extends to $\beta = 1035$ and 11240, but the good in-line force predictions do suggest this. That the predicted wake formations are less transverse for $\beta = 11240$ than for $\beta = 1035$ is associated with turbulent separation occurring further downstream, as is the case for supercritical Reynolds numbers in steady incident flow.

5. Discussion

The basic premise of an unsteady RANS flow solver is that large-scale fluctuations, whether due to vortex shedding or imposed oscillation, are of sufficiently large scale to be distinct from small-scale turbulence which is modelled. A further assumption made here is that large-scale flow structures are 2-D. The flows investigated only approximate this to a variable degree, and we rely on experimental evidence to define spanwise correlation. This will remain the case until 3-D computations are a practical possibility at these high Reynolds numbers. The nonlinear eddy-viscosity model of

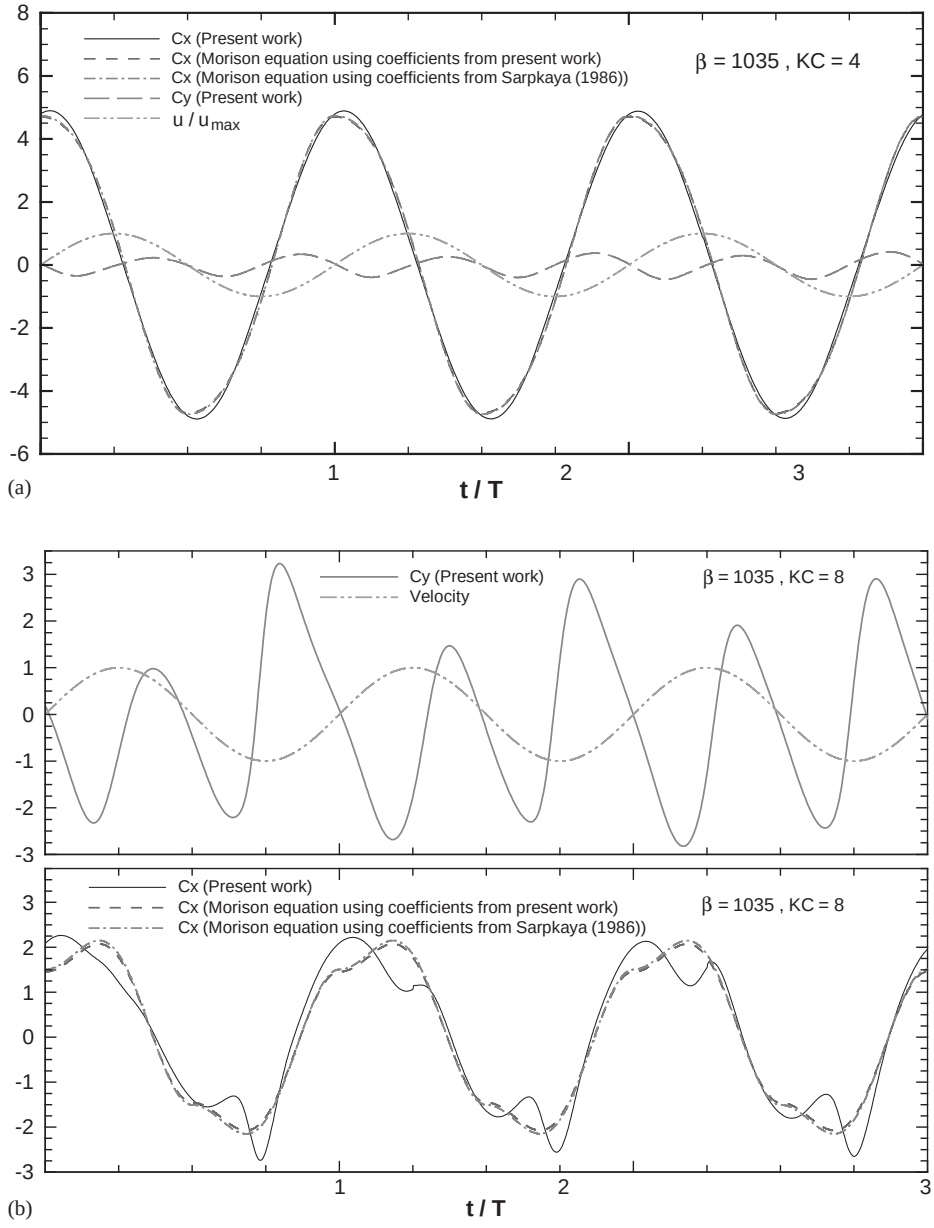

Fig. 10. (a) Variation of in-line force coefficient C_x and lift coefficient C_y with time for KC = 4 and $\beta = 1035$, using the present modified CLS model. (b) Variation of in-line force coefficient C_x and lift coefficient C_y with time for KC = 8 and $\beta = 1035$, using the present modified CLS model. (c) Variation of in-line force coefficient C_x and lift coefficient C_y with time for KC = 12 and $\beta = 1035$, using the present modified CLS model. (d) Variation of in-line force coefficient C_x and lift coefficient C_y with time for KC = 15 and $\beta = 1035$, using the present modified CLS model.

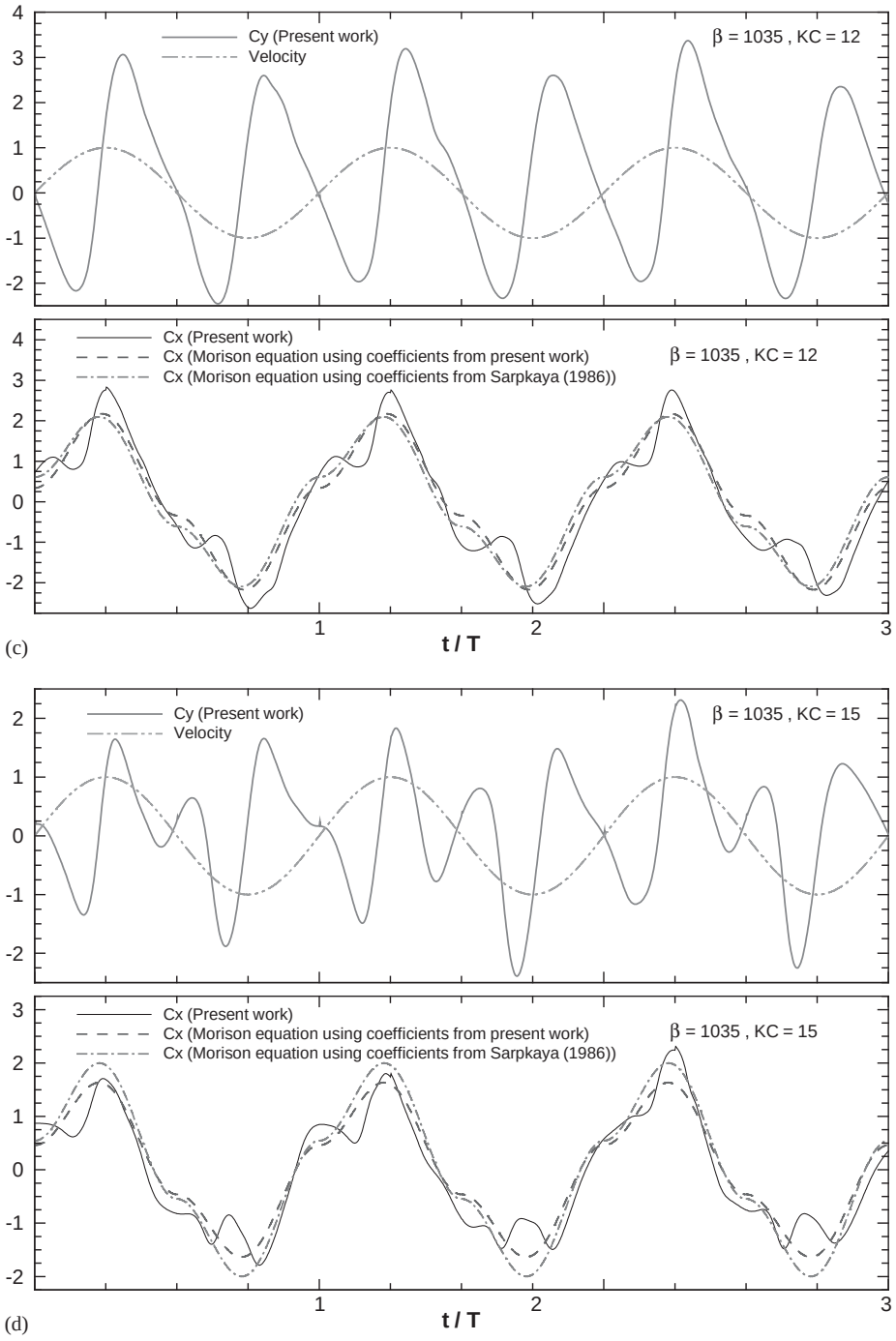

Fig. 10 (*continued*).

Craft et al. (CLS) with reduced coefficients for cubic terms was the most successful of those applied. It has also been found to be a suitable choice for unsteady compressible flows around lifting aerofoils (Barakos and Drikakis, 2000), although no modification of the original coefficients was attempted in that case.

Some results using the linear LS (industry-standard) $k-\varepsilon$ model have been presented and reinforce well-known limitations. Quadratic terms are necessary to resolve normal stress anisotropy and cubic terms account for effects due to

curvature and strain. In the CLS model, the low-Reynolds-number elements in the cubic terms are set up to resolve flows with complex strain with sensitivity to viscous effects. The coefficients of these terms are reduced for these flows following the suggestion for the model of LCL. The model is suited to flows with transition, curvature and separation, which occur here. It is known that the CLS model predicts transitional flat plate flows subjected to adverse pressure

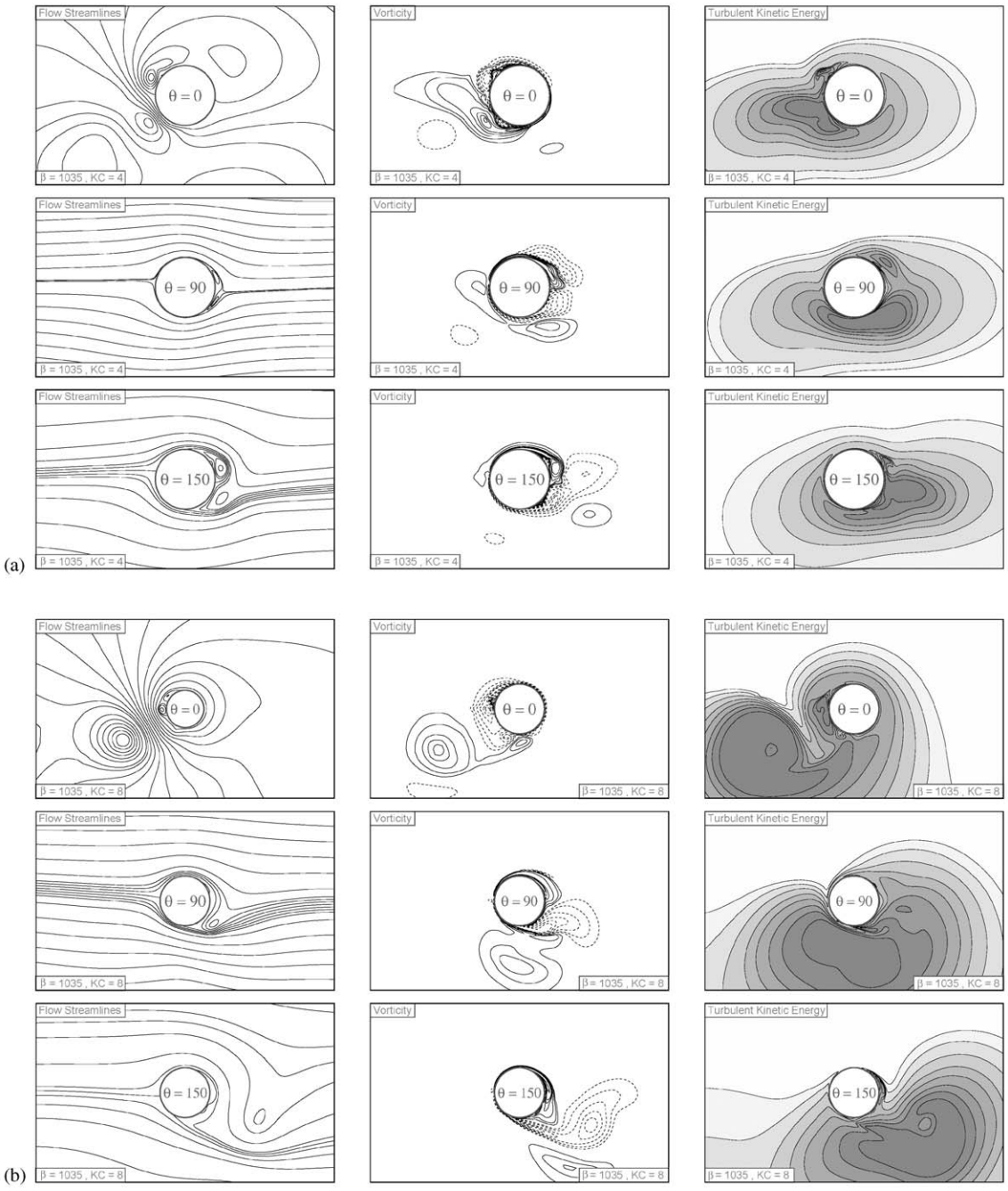

Fig. 11. (a) Plots of streamlines, vorticity contours and k contours at different phases θ for KC = 4 and $\beta = 1035$. (b) Plots of streamlines, vorticity contours and k contours at different phases θ for KC = 8 and $\beta = 1035$. (c) Plots of streamlines, vorticity contours and k contours at different phases θ for KC = 12 and $\beta = 1035$. (d) Plots of streamlines, vorticity contours and k contours at different phases θ for KC = 15 and $\beta = 1035$.

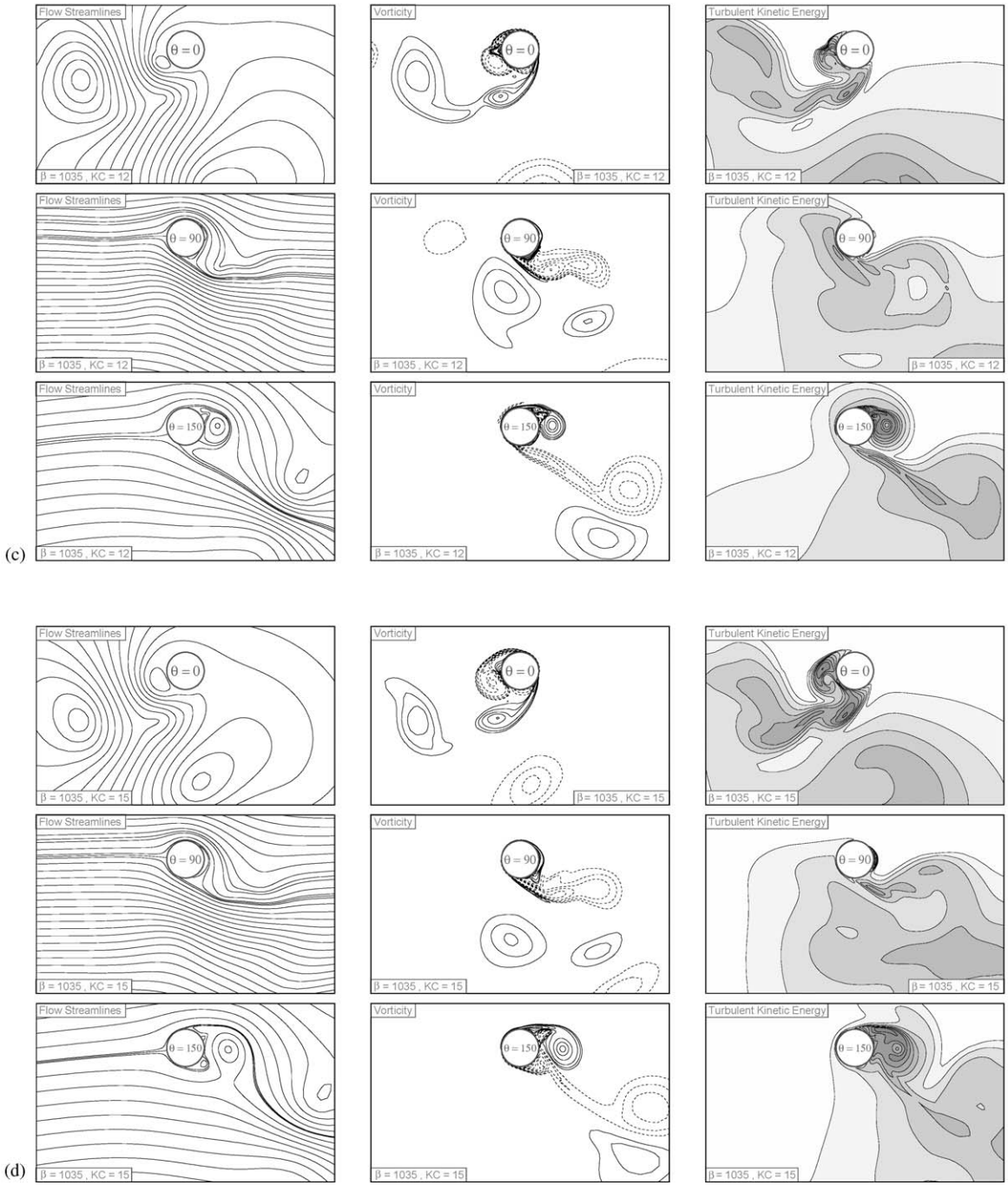

Fig. 11 (*continued*).

gradients, and cubic terms account for the influence of a curved surface. Of course, the ability to predict such transition does not extend to the effect of coherent transitional structures like the Honji instability in oscillatory flow. It should also be noted that purely flat-plate transition (without separation) would occur at $KC \simeq 17$ for $\beta = 1035$ and $KC \simeq 5$ for $\beta = 11240$. Analysis of resulting forces and discussion are given in Cobbin et al. (1995). Interestingly, it would appear that Honji instability is a relatively low β-number phenomenon, as transition actually occurs at a lower KC value than that for Honji instability at $\beta = 11240$. This KC value is well below 5, indicating the strong influence of curvature on

transition. That there is some effect of turbulence in the model at KC = 0.5 for $\beta = 1035$ (when laminar flow is expected) indicates that the CLS model overestimates the influence of curvature on transition. In steady incident flow, a clear further weakness of the model lies in its inability to simulate attached separation bubbles with turbulent re-attachment and then turbulent separation at critical Reynolds numbers.

The predictions of in-line force (defined by C_D and C_M) for KC < 2, approximately, are less satisfactory than for 3-D LES computations (Lu et al., 1997), probably because of the enforced two dimensionality (although problems associated with transition and curvature apply to both approaches). Also the CLS model is set up for steady incident flow with large-scale separation and at these KC values there are complex thin (small-scale) wakes and re-attachment (as well as transition on a curved surface). The basic premise for unsteady RANS modelling must be doubtful. The turbulence model is better suited for force predictions at higher KC values, where there is more prominent separation with larger scale vortex shedding. Predictions are generally reasonable (for KC < 18 where vortex shedding is thought to be 2-D) and at a much higher $\beta = 11240$ than has been attained previously.

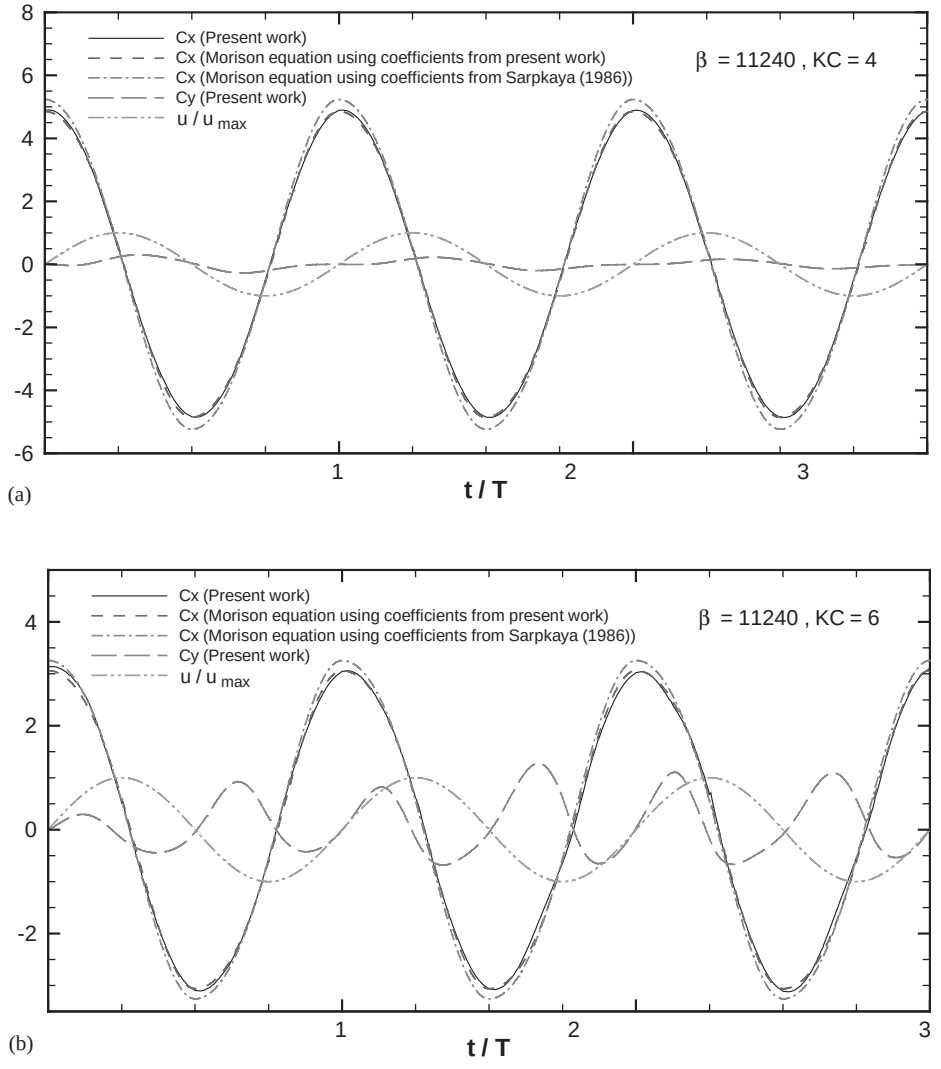

Fig. 12. (a) Variation of in-line force coefficient C_x and lift coefficient C_y with time for KC = 4 with $\beta = 11240$ using the present modified CLS model. (b) Variation of in-line force coefficient C_x and lift coefficient C_y with time for KC = 6 with $\beta = 11240$ using the present modified CLS model. (c) Variation of in-line force coefficient C_x and lift coefficient C_y with time for KC = 10 with $\beta = 11240$ using the present modified CLS model. (d) Variation of in-line force coefficient C_x and lift coefficient C_y with time for KC = 15 with $\beta = 11240$ using the present modified CLS model. (e) Variation of in-line force coefficient C_x and lift coefficient C_y with time for KC = 20 with $\beta = 11240$ using the present modified CLS model.

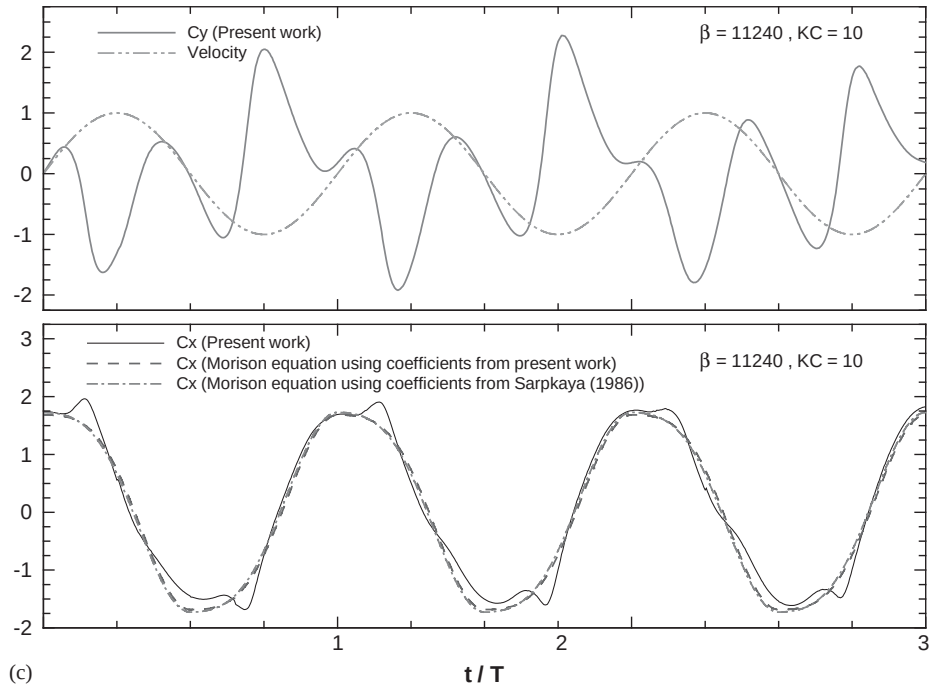

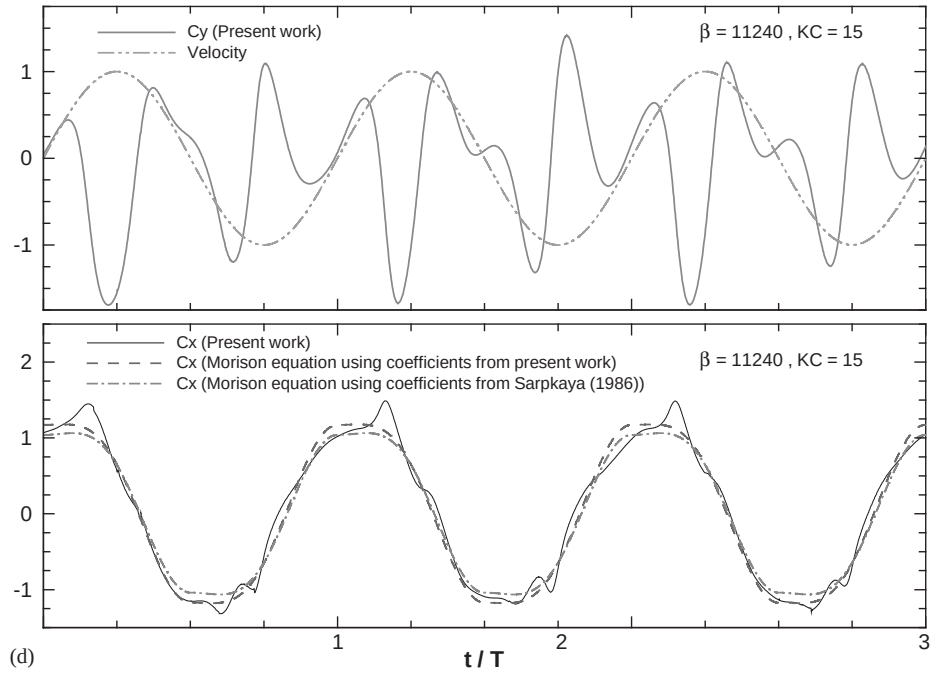

Fig. 12 (*continued*).

Some new insights in oscillatory flow are gained. That C_D and $C_{L\max}$ are much smaller for $\beta = 11240$ than for $\beta = 1035$, when vortex shedding occurs, is because separation is delayed due to turbulence, forming a narrower wake with reduced transverse structures. It thus seems that this is not due to more strongly 3-D vortex shedding at a higher β value, as might be intuitively expected (as the simulation is 2-D). $C_{L\max}$ can be greater than the in-line force for $\beta = 11240$ as it was for $\beta = 1035$.

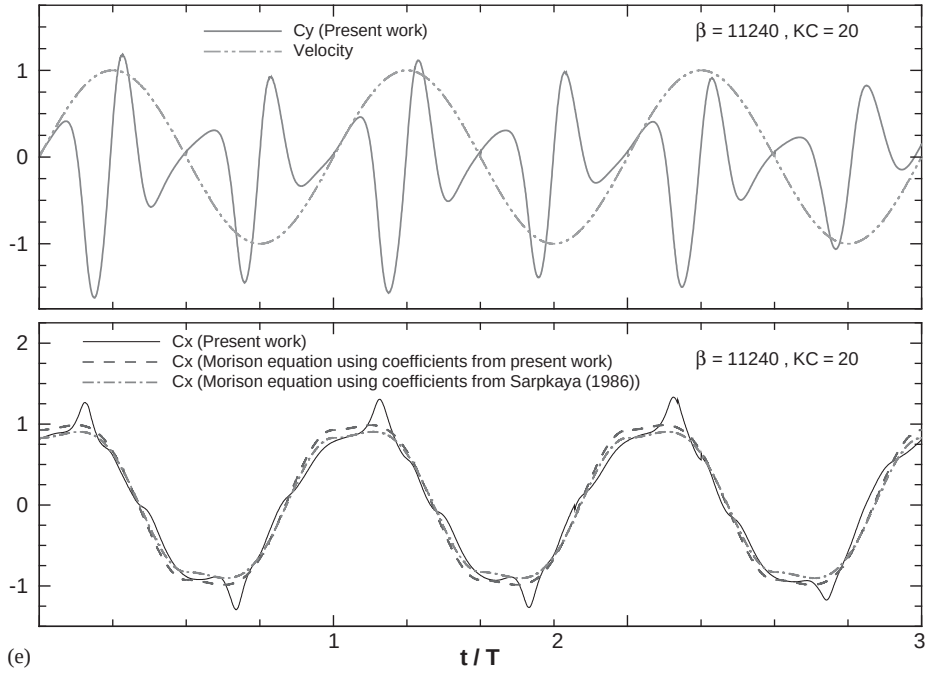

Fig. 12 (*continued*).

For steady ambient flow, $C_{L\,\mathrm{r.m.s.}}$ is generally in approximate agreement with or slightly greater than sectional (local) force measurements at subcritical Reynolds numbers, although not with those measured over several diameters, due to poor spanwise correlation. Corresponding sectional lift forces have not been measured at supercritical (or critical) Reynolds numbers, but the computational modelling indicates that these would be of similar magnitude to those at subcritical Reynolds numbers. Experimental data for supercritical Reynolds numbers is generally quite sparse. Comparison with the modelling raises questions concerning the precise experimental conditions, in relation to free-stream turbulence and/or surface roughness, where tiny effects could be significant. This is suggested because comparisons with linear (LS) modelling are quite close and it is well known that such models overgenerate turbulence near stagnation quite substantially; roughness and/or free-stream turbulence would have a similar effect.

Finally, it is pertinent to ask whether LES would give better predictions with large-scale vortex shedding. It is of course 3-D, and so cellular spanwise structures should be simulated (and indeed have been at subcritical Reynolds numbers). However, the near-wall turbulence modelling is generally based on a mixing-length type formulation with damping functions. This cannot represent transition. Thus it seems that a nonlinear cubic eddy-viscosity model of the CLS type offers the best option for certain categories of flow (given that DNS will remain impractical at these Reynolds numbers without a change in computer technology). Such modelling for near-wall flows could be combined with LES for the outer flow where subgrid modelling becomes appropriate.

Most of the runs undertaken here required about 20 h on a 1.3 GHz PC. Codes were written in Visual Fortran.

6. Conclusions

A 2-D RANS equation solver with the nonlinear eddy viscosity model of Craft et al. (1996) has been used to predict forces in steady and oscillatory flows past a circular cylinder for a wide range of Reynolds numbers, involving laminar and turbulent separation. Prediction of experimental results for steady incident flow with large-scale vortex shedding is optimised with the coefficients of cubic terms reduced by 60%, suggested previously by Lien et al. (1996). The critical Reynolds number of 2×10^5 is predicted and forces are in reasonable agreement with experiment up to this value. The inability to predict attached separation bubbles is however a marked weakness. At supercritical Reynolds numbers, there is some agreement but considerable scatter in experimental data. Forces in complex oscillatory

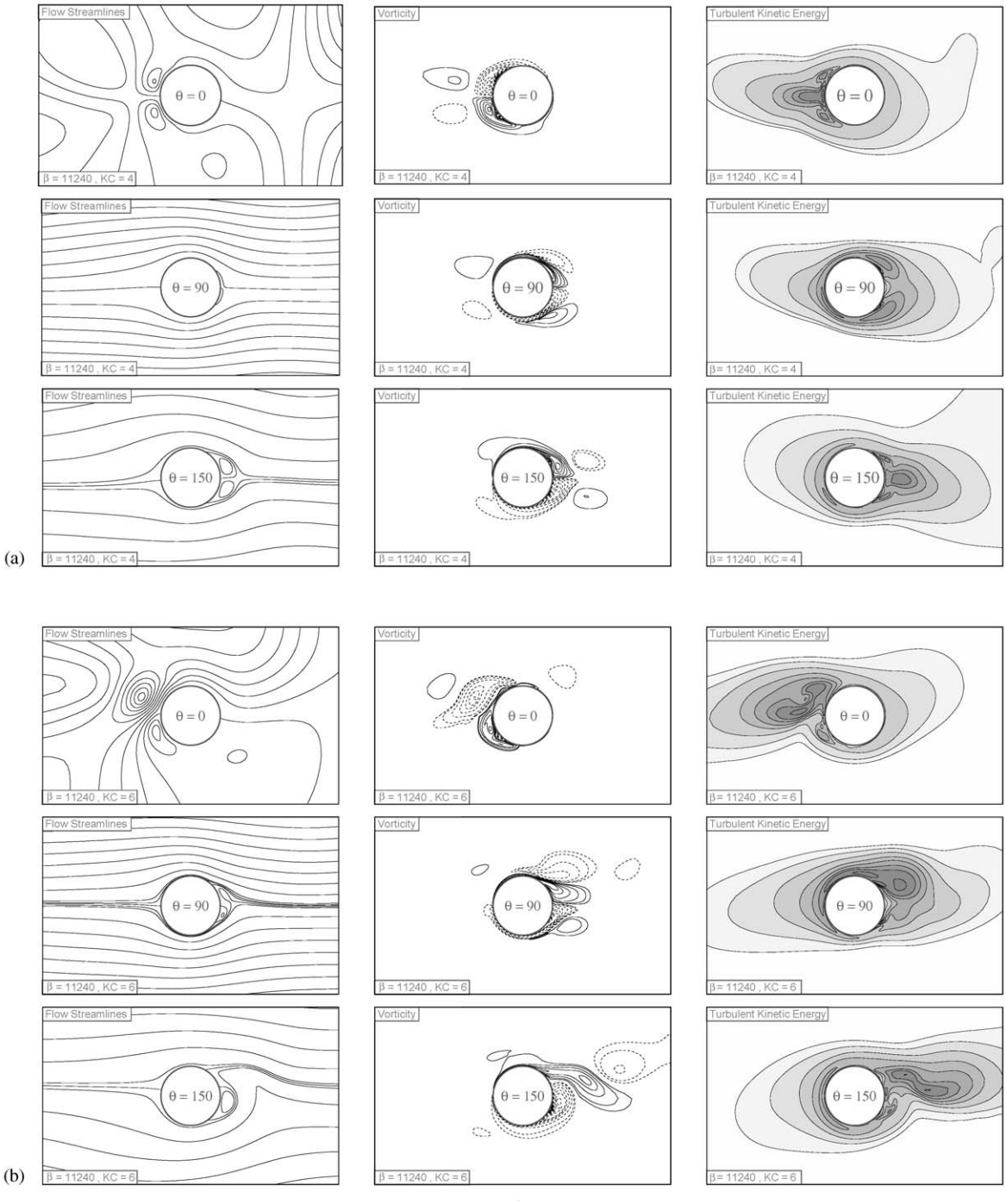

Fig. 13. (a) Plots of streamlines, vorticity and k/U_0^2 contours at different phases for KC = 4 and $\beta = 11240$. (b) Plots of streamlines, vorticity and k/U_0^2 contours at different phases for KC = 6 and $\beta = 11240$. (c) Plots of streamlines, vorticity and k/U_0^2 contours at different phases for KC = 10 and $\beta = 11240$. (d) Plots of streamlines, vorticity and k/U_0^2 contours at different phases for KC = 15 and $\beta = 11240$. (e) Plots of streamlines, vorticity and k/U_0^2 contours at different phases for KC = 20 and $\beta = 11240$.

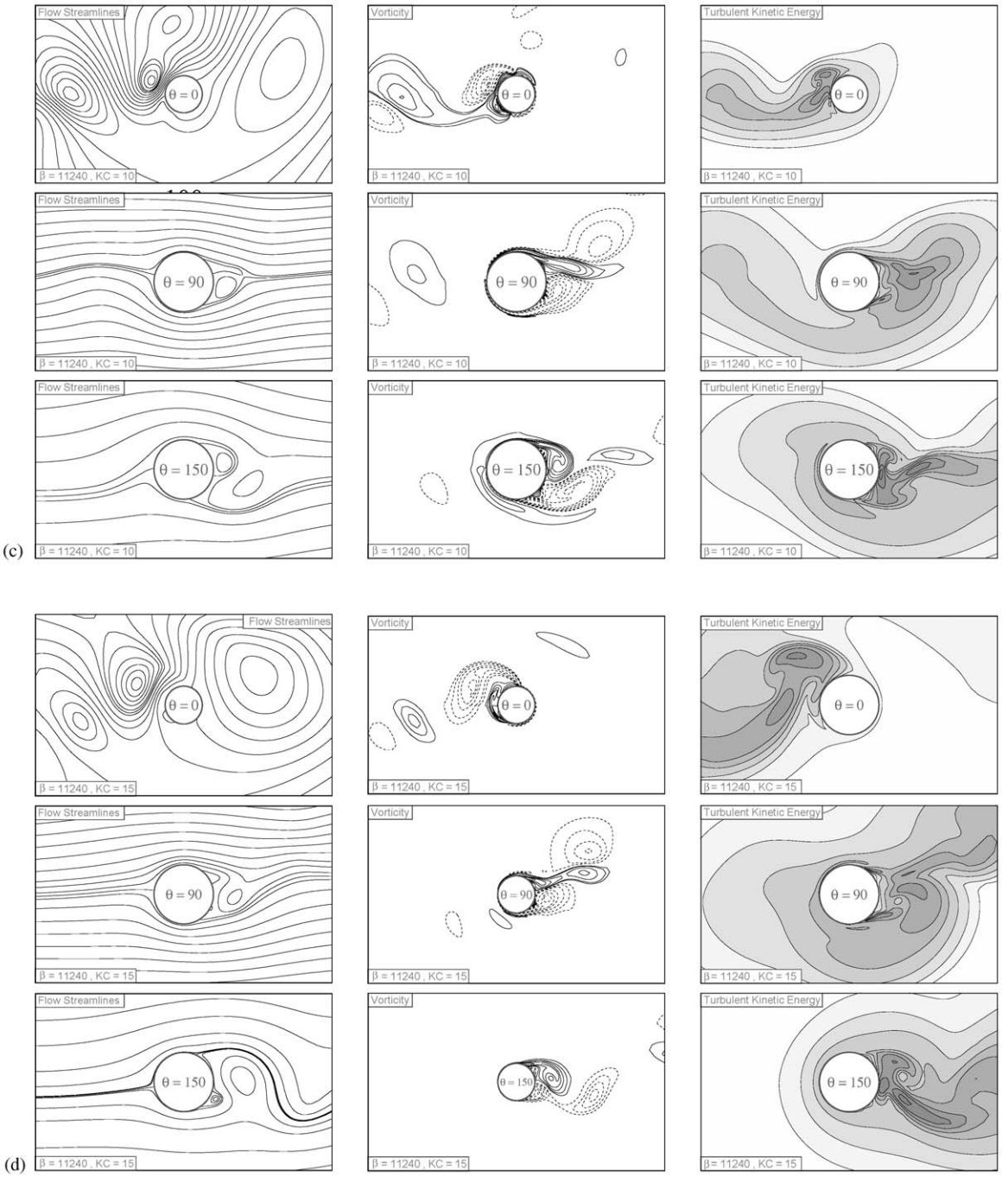

Fig. 13 (*continued*).

flows at high β values are predicted reasonably for $KC > 2$, approximately, where vortex shedding is prominent, and $KC < 18$, where real flows are thought to be almost two dimensional. For $KC < 2$, where wakes are thin and of a small scale, prediction is less satisfactory than for LES (Lu et al., 1997). Differences in wake formation between $\beta = 1035$ and 11240 are demonstrated, due to the more prominent effects of turbulence for the latter. For $\beta = 1035$ vortex pairing forms transverse wakes while for $\beta = 11240$ vortex pair convection is more in line with the flow direction.

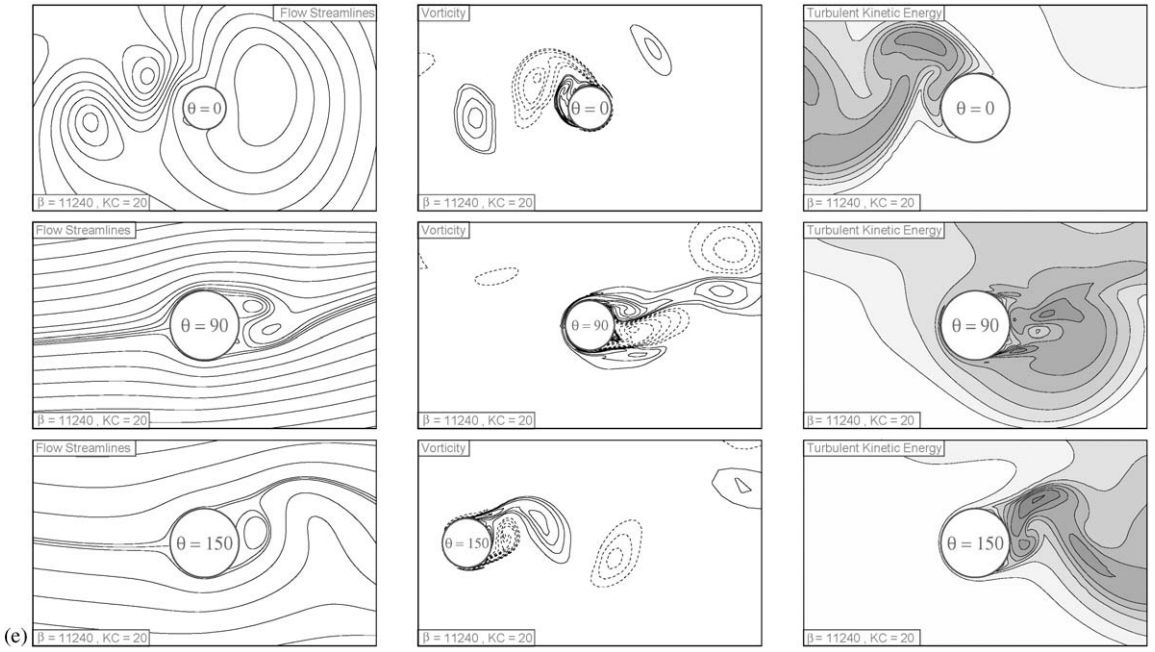

Fig. 13 (*continued*).

Acknowledgements

Support from the Ministry of Science in Iran and from EPSRC ROPA Grant GR/M96018 are gratefully acknowledged.

References

Achenbach, E., 1968. Distribution of local pressure and skin friction around a circular cylinder in cross-flow up to $Re = 5 \times 10^6$. Journal of Fluid Mechanics 34, 625–639.

Apsley, D.D., Chen, W.-L., Leschziner, M.A., Lien, F.-S., 1997. Nonlinear eddy viscosity modelling of separated flows. Journal of Hydraulics Research 35, 723–748.

Barakos, G.N., Drikakis, D., 2000. Unsteady separated flows over manoeuvring lifting surfaces. Philosophical Transactions of the Royal Society A 358, 3279–3291.

Bearman, P.W., Russell, M.P., 1996. Measurements of hydrodynamic damping of bluff bodies with application to the prediction of viscous damping of TLP hulls, Proceedings of the 21st Symposium on Naval Hydrodynamics, Trondheim, Norway.

Breuer, M., 1998. Large eddy simulation of the subcritical flow past a circular cylinder: numerical and modelling aspects. International Journal Numerical Methods in Fluids 28, 1281–1302.

Celik, I., Shaffer, F.D., 1995. Long time-averaged solutions of turbulent flow past a circular cylinder. Journal of Wind Engineering and Industrial Aerodynamics 56, 185–212.

CIRIA, 1977 (Construction Industry Research and Information Association). Report UR8, Dynamics of Marine Structures, London.

Cobbin, A.M., Stansby, P.K., Duck, P.W., 1995. The hydrodynamic damping force on a cylinder in oscillatory, very high Reynolds number flows. Applied Ocean Research 17, 291–300.

Craft, T.J., Launder, B.E., Suga, K., 1996. Development and application of a cubic eddy-viscosity model of turbulence. International Journal of Heat and Fluid Flow 17, 108–115.

Craft, T.J., Gant, S.E., Iacovides, H., Launder, B.E., 2001. Development and application of a new wall function for complex flows. ECCOMAS (European Community on Computational Methods in Applied Sciences) CFD Conference, Swansea.

Ferziger, J.H., Peric, M., 1996. Computational Methods for Fluid Dynamics. Springer, Berlin.

Honji, H., 1981. Streaked flow around an oscillating circular cylinder. Journal of Fluid Mechanics 107, 509–520.

Karniadakis, G.E., Triantafyllou, G.S., 1992. Three-dimensional dynamics and transition to turbulence in the wake of bluff objects. Journal of Fluid Mechanics 238, 1–30.

Keulegan, G.H., Carpenter, L.H., 1958. Forces on cylinders and plates in an oscillating fluid. National Bureau Standards Journal of Research 60, 423–440.

Launder, B.E., Sharma, B.I., 1974. Application of the energy-dissipation model of turbulence to the calculation of flow near a spinning disc. Letters in Heat and Mass Transfer 1, 131–138.

Letherman, S.B., Cotton, M.A., Stansby, P.K., Chen, C., Chen, D., 2000. An assessment of $k-\varepsilon$ and $k-l$ turbulence models for a wide range of oscillatory rough bed flows. Journal of Hydroinformatics 2, 221–234.

Lien, F.S., Chen, W.L., Leschziner, M.A., 1996. Low-Reynolds-number eddy-strain-viscosity modelling based on non-linear stress–strain/vorticity relations. In: Proceedings of the Third International Symposium of Engineering Turbulence Modelling and Measurements, Crete.

Lu, X., Dalton, C., Zhang, J., 1997. Application of large eddy simulation to an oscillating flow past a circular cylinder. ASME Journal of Fluids Engineering 119, 519–525.

Murakami, S., Iizuka, S., 1999. CFD analysis of turbulent flow past square cylinder using dynamic LES. Journal of Fluids and Structures 13, 1097–1112.

Norberg, C., 2001. Flow around a circular cylinder: aspects of fluctuating lift. Journal of Fluids and Structures 15, 459–469.

Obasaju, E.D., Bearman, P.W., Graham, J.M.R., 1988. A study of forces, circulation and vortex patterns around a circular cylinder in oscillating flow. Journal of Fluid Mechanics 196, 467–494.

Prandtl, L., 1927. Über die ausgebildete turbulenz. Zeitschrift fuer Angewandte Mathematik und Mechanik 5, 137–138.

Rodi, W., Ferziger, J.H., Breuer, M., Porquie, M., 1996. Status of large eddy simulation: results of a workshop. ASME Journal of Fluids Engineering 119, 248–262.

Roshko, A., 1961. Experiments on the flow past a circular cylinder at very high Reynolds number. Journal of Fluid Mechanics 10, 345–356.

Sani, R.L., Gresho, P.M., 1994. Resumé and remarks on the open boundary condition minisymposium. International Journal Numerical Methods in Fluids 18, 983–1008.

Sarpkaya, T., 1976. Vortex shedding and resistance in harmonic flow about smooth and rough circular cylinders at high Reynolds numbers. Naval Postgraduate School Report NPS-59SL76021, Monterey, California.

Sarpkaya, T., 1986. Force on a circular cylinder in viscous oscillatory flow at low Keulegan–Carpenter numbers. Journal of Fluid Mechanics 165, 61–71.

Schewe, G., 1983. On the force fluctuations acting on a circular cylinder in crossflow from subcritical up to transcritical Reynolds numbers. Journal of Fluid Mechanics 133, 265–285.

Smith, P.A., Stansby, P.K., 1989. Postcritical flow around a circular cylinder by the vortex method. Journal of Fluids and Structures 3, 275–291.

Speziale, C.G., 1987. On nonlinear $k-l$ and $k-\varepsilon$ models of turbulence. Journal of Fluid Mechanics 178, 459–475.

Stansby, P.K., 1974. Vortex wakes of cylinders oscillating in uniform and sheared flows. Ph.D. Dissertation, University of Cambridge.

Stansby, P.K., Slaouti, A., 1993. Simulation of vortex shedding including blockage by the random-vortex and other methods. International Journal Numerical Methods in Fluids 17, 1003–1013.

Szepessy, S., 1993. On the control of circular cylinder flow by end plates. European Journal of Mechanics, B/Fluids 12 (N2), 217–244.

Wang, C.Y., 1968. On high frequency oscillating viscous flows. Journal of Fluid Mechanics 32, 55–68.

Williamson, C.H.K., 1985. Sinusoidal flow relative to circular cylinders. Journal of Fluid Mechanics 155, 141–174.

Williamson, C.H.K., 1996. Three-dimensional wake transition. Journal of Fluid Mechanics 328, 345–407.